Int. J. Heat Mass Transfer. Vol. 31, No. 11, pp. 2291–2304, 1988
Printed in Great Britain

0017–9310/88 $3.00 + 0.00

Experimental studies of critical heat flux for low flow of water in vertical annuli at near atmospheric pressure

MOHAMED S. EL-GENK, STANLEY J. HAYNES and SUNG-HO KIM
Department of Chemical and Nuclear Engineering, University of New Mexico, Albuquerque, NM 87131, U.S.A.

(*Received* 20 *October* 1987 *and in final form* 13 *April* 1988)

Abstract—Experiments are performed to measure the critical heat flux (CHF) for low flow of water in vertical annuli near atmospheric pressure (0.118 MPa). CHF data are collected for water inlet subcooling ranging from 44 K (or 182 kJ kg^{-1}) to 75 K (or 312 kJ kg^{-1}), and mass fluxes from 0 to 260 kg m^{-2} s^{-1}. The CHF values vary from 155 kW m^{-2} for zero inlet flow to a maximum of 1418 kW m^{-2} for a water mass flux of 260 kg m^{-2} s^{-1}. The data are classified and correlated according to the flow transition which occurred at CHF. Two CHF correlations are developed, one for the slug–churn and the churn–annular flow transitions and the other for the annular–annular mist flow transition. The heat flux at incipient flow chugging is also measured and found to vary from a minimum of about 40% of the CHF values in the smallest annulus (annulus ratio = 1.575) to a maximum of approximately 88% of CHF in the other larger annuli (annulus ratio = 1.72 and 2.0). Results also show that the heat flux at incipient chugging increases as either the water mass flux or inlet subcooling increases. The CHF values for zero inlet flow are predicted within ±25% using Block and Wallis' flooding correlation.

INTRODUCTION

CRITICAL heat flux (CHF) is a phenomenon which results in a build up of an insulating vapor layer on the heater's surface. This vapor layer causes an abrupt reduction in the heat transfer rate and a simultaneous, precipitous rise in the heater's surface temperature. This rise in the heater's surface temperature could be enough to cause material failure of the heater.

The CHF (or the boiling crisis) phenomena can generally be classified into two broad categories depending on the vapor quality. The first, departure from nucleate boiling (DNB), usually occurs at a low vapor quality typical of that encountered at high pressure and/or high coolant mass velocities. This type of CHF phenomenon noted by a transition from nucleate boiling to film boiling associated with an abrupt increase in the heater's surface temperature. Several conditions leading to the occurrence of the DNB type CHF have been proposed by Tong [1], and recently by Hewitt [2], Collier [3] and Katto [4]. The second category of the CHF phenomena is dryout CHF, which is commonly referred to as Harwell's model because it was first postulated by Harwell scientists [5]. This type of CHF usually occurs at high vapor quality or void contents typical of those occurring in constrained geometries and at saturated or near saturated flow conditions. Prior to the boiling crisis, the heater's surface is covered by a thin layer of liquid, while the bulk of the coolant flow consists of a mixture of vapor and entrained liquid droplets. The heat flow through the liquid film induces evaporation at the surface of the liquid layer the thickness of which decreases as the heat flux increases. The thickness of this liquid film is also influenced by the phenomena of liquid droplet entrainment and deposition. When the heat flux is high enough to evaporate the liquid film, the surface dries out, causing an abrupt rise in the heater's surface temperature. The values of the dryout type CHF as well as the heater's surface temperature at CHF are lower than those for the DNB type CHF. The flow pattern observed in the dryout type CHF is generally an annular or an annular mist type flow. Extensive reviews of the scenarios leading to the occurrence of the dryout type CHF have been presented by several authors [2–7]; however, there has been little direct experimental study of these scenarios for low flow and low pressure conditions.

Although many CHF correlations are available for multi-rod bundles and for annuli and tubes, these correlations were developed based on mostly high flow rate and high pressure data [8–11]. Consequently, using these correlations to predict CHF values at lower flow rates and low pressures would be inappropriate. Biasi *et al.* [8], have developed two CHF correlations; one was based on low vapor exit quality data and the other was based on high exit vapor quality data. These correlations covered a wide range of pressure (0.27–14.2 MPa) and mass fluxes (100–6000 kg m^{-2} s^{-1}) for various tube diameters and lengths (D = 0.003–0.0375 m and L = 0.2–0.6 m). Similar to Biasi *et al.* [8], Macbeth [9, 10] has developed two correlations, one for low mass fluxes and the other for high mass fluxes. The range of the water mass fluxes for these correlations varied from 13.6 to 12 232

NOMENCLATURE

A	cross-sectional flow area [m^2]
A_h	heated surface area [m^2]
D	diameter [m]
D_e	equivalent diameter based on wetted perimeter [m]
D_{eh}	equivalent diameter based on heated perimeter [m]
g	gravitational acceleration [$m\,s^{-2}$]
G	water mass flux [$kg\,m^{-2}\,s^{-1}$]
G^*	dimensionless mass flux, equation (1), $G/\sqrt{(\lambda\rho_v g\Delta\rho)}$
h_i	inlet water enthalpy [$kJ\,kg^{-1}$]
h_f	saturated water enthalpy [$kJ\,kg^{-1}$]
h_{fg}	latent heat of vaporization [$kJ\,kg^{-1}$]
Δh_i	$h_f - h_i$ [$kJ\,kg^{-1}$]
j	drift velocity [$m\,s^{-1}$]
L	length of heated section [m]
$\dot{m}$	water mass flow rate [$kg\,s^{-1}$]
$N_{\mu f}$	dimensionless viscosity, equation (6), $[\mu_f/(\rho_f\sigma\sqrt{(\sigma/\Delta\rho g)})^{1/2}]$
P	pressure [MPa]
Q	total power [kW]
q^*	dimensionless CHF, equation (1), $q_c''/h_{fg}\sqrt{(\lambda\rho g\Delta\rho)}$
q_c''	critical heat flux [$kW\,m^{-2}$]
Re_f	film Reynolds number, equation (7), $4\Gamma/\nu_f$.

Greek symbols

Γ	volumetric flow rate per wetted perimeter, equation (8) [$m^2\,s^{-1}$]
δ_f	thickness of liquid film [m]
ε	annulus ratio, D_o/D_i
λ	coefficient, equation (1), $\sqrt{(\sigma/g\Delta\rho)}$
μ	dynamic viscosity [$kg\,m^{-1}\,s^{-1}$]
ν	kinematic viscosity [$m^2\,s^{-1}$]
ρ	density [$kg\,m^{-3}$]
$\Delta\rho$	$\rho_f - \rho_v$ [$kg\,m^{-3}$]
σ	water surface tension [$N\,m^{-1}$].

Subscripts

f	liquid
i	inner heated tube
o	outer wall
v	vapor.

$kg\,m^{-2}\,s^{-1}$. However, the low mass flux correlation, which is of interest to the present work, employed only six CHF data points at 0.104 MPa; the rest of the 372 data points were for a system pressure between 0.24 and 13.8 MPa. For subcooled flow conditions in tubes, annuli, and multi-rod bundles, Bernath [11] has developed a CHF correlation based on data taken at system pressures ranging from 0.104 to 20.68 MPa and for coolant mass fluxes ranging from 750 to 5000 $kg\,m^{-2}\,s^{-1}$. Because of their limited data base at low flow, the applicability of the Macbeth and Bernath correlations to low flow, low pressure conditions is questionable.

Other research has shown that for a given inlet subcooling while the CHF increases precipitously with the coolant mass flow velocity at low mass flow rate, it increases at a much lower rate at higher coolant mass flow rates [3]. The coolant mass flux at the transition from the low to the high flow CHF regimes is independent of geometry. This transition was reported to occur in vertical tubes at about 200 kg $m^{-2}\,s^{-1}$ [12], and in vertical annuli at about 180 kg $m^{-2}\,s^{-1}$ [13]. The difference between these transition values of tubes and annuli is insignificant considering possible experimental errors and judgements involved in establishing the transition values. Another major difference between the low flow and high flow CHF regimes is that in the high flow regime the CHF values strongly depend on the inlet subcooling; conversely, in the low flow regime the CHF values are nearly independent of the inlet subcooling.

The only consistent CHF data for low flow of water in vertical annuli at near atmospheric pressure were those reported by Rogers *et al.* [13], and Mishima and Ishii [14]. Rogers *et al.* [13] collected CHF data for upward flow of water in vertical annuli (annulus ratios of 1.68, 1.91, and 2.31) for both subcooled and saturated conditions. The water mass fluxes ranged from 60 to 1200 kg $m^{-2}\,s^{-1}$ with the majority of the data being collected at mass fluxes greater than 180 kg $m^{-2}\,s^{-1}$; the CHF data were collected at water mass fluxes less than 180 kg $m^{-2}\,s^{-1}$ in only one annulus, $\varepsilon = 1.68$. In these experiments [13] the CHF occurred as a large vapor slug passed through the top of the heated section; however, the flow transition at CHF was not investigated. The CHF correlations developed by Rogers *et al.*, based on the linearity exhibited by the data between the CHF and the inlet subcooling for mass fluxes higher than 180 kg $m^{-2}\,s^{-1}$, were entirely empirical. Because the constants of the correlations were determined individually for each annulus, the correlations could not be applied to other annular geometries [13].

Mishima and Ishii [14] related their CHF data to the flow transition (churn–annular flow) which occurred at CHF. They identified the flow transition at CHF in two ways: by plotting the CHF values vs the equilibrium exit quality on a two-phase flow map and by visual observations. However, the data base obtained was limited since these experiments were confined to only one annulus, $\varepsilon = 1.27$, and to very low water mass fluxes (from 0 to 40 kg $m^{-2}\,s^{-1}$). Mishima and Ishii [14] correlated their CHF data using a drift flux model transition criterion from churn

flow to annular flow and assuming that the void distribution coefficient in the annulus was the same as in a vertical tube [15]. This assumption, which implies that the maximum void concentration occurs at the center of the tube, may not be applicable for flow in vertical annuli because of the unheated outer wall and the lack of geometrical symmetry of the void distribution in the annular gap.

To broaden the available CHF data base for low flow of water at near atmospheric pressure, this work collected CHF data using three vertical annuli and investigated the effects of the annulus ratio, water mass flux and inlet subcooling on the values of CHF. The CHF data were correlated and the correlations compared with those of Macbeth and Bernath to assess their applicability for predicting CHF values at low flow and near atmospheric conditions.

EXPERIMENTAL SETUP

The CHF test section consists of a 304 stainless steel inner tube, as the heating element, placed inside unheated Pyrex tubes of various diameters. The stainless steel tube is 50 cm long, 1.27 cm o.d. and has a 0.889 mm wall thickness. This tube is silver brazed to a 1.27 cm diameter, 15 cm long brass rod at the top and to a 1.27 cm o.d., 15 cm long brass tube at the bottom. The brass tube provides access to the interior of the stainless steel heated tube for temperature measurements. The other ends of the brass tube and the brass rod were screwed into 4 cm o.d. and 22 cm long copper conductors for connecting the stainless steel tube to the d.c. power generator. The copper conductors have 15 mm longitudinal central holes, which provide access for monitoring temperatures at the heated tube's inner surface.

The total electric resistivity of the brass rod, brass tube, copper connectors and the electric cables was small when compared to that of the stainless steel tube ($<7\%$ of the total resistivity of the circuit); however, the values of CHF were determined based solely on the resistivity of the stainless steel tube. The water inlet temperature was finely controlled by using a Chromalox Type ARTM water immersion heater.

Temperature measurements in the CHF experiments were made at eight axial locations at the inner surface of the stainless steel tube (1, 3, 5, 10, 20, 30, 40 and 45 cm from the top of the heated length) and also at five other locations in the loop. The coolant temperatures in the loop were recorded at the inlet and the outlet of the preheater, in the upper and lower headers, and at the outlet of the riser (1.7 m long) which was connected to the bottom of the overhead tank.

A special probe was developed for measuring the temperature of the inner surface of the heated tube. The temperature probe had a Teflon former, 0.95 cm o.d. and 50 cm long, with 8 radial holes (5 mm diameter and 4 mm deep) located at 1, 3, 5, 10, 20, 30, 40 and 45 cm from the top of the probe. Each hole is rotated 45° counter-clockwise from the location above to keep the thermocouple leads separated. In each hole, a spring loaded plunger was placed to house the thermocouple junction. The pressure exerted by the compression spring on the plunger kept the thermocouple junction in contact with the inner surface of the heated tube during the experiments. Each thermocouple lead was laid in a longitudinal groove which originated at a radial hole (measuring point) and terminated at the bottom of the probe. Except for the sensing ends of the thermocouples, the Teflon former assembled with thermocouples was insulated from the inner surface of the heater with 0.8 mm thick Teflon spaghetti tubing. The temperatures at the outer surface of the heated tube were then determined. These temperatures were based on the temperatures measured at the inner surface after accounting for the temperature drop across the wall (<0.5 K) and the contact resistance between the thermocouple junctions and the tube wall (approximately 0.1 K).

Temperature measurements in the experiments were made using type-K, OMEGA brand thermocouples. When calibrated, the thermocouple measurements were in excellent agreement (within $\pm 0.2\%$) with the tabulated values in the *OMEGA Temperature Handbook* over the temperature range from 283 up to 800 K. The electric power was supplied to the test section by a Sel-Rex 200 kW (100 V, 2000 A) d.c. power generator. The voltage and the current values, monitored directly by the data acquisition system, were accurate to within ± 0.001 V and ± 13.5 A, respectively. As a result, the uncertainties in the electric power supply to the test section varied from 0.9% at the high CHF values to 1.9% at the low CHF values and the uncertainties in the measured CHF values from 2.7% at the higher power levels to 4.2% at the low power levels.

The recording of all temperatures, power, and flow measurements was fully automated through the data acquisition system which consisted of a HP-3497A data logger, an OMEGALINE 620 chart recorder, and an IBM-9000 CS computer for storage and analysis of data. The water inlet flow rate was measured using a Flow Technology brand (Model FR-6-8N5-LJC(S)) pulse type turbine flow meter which was calibrated for the range from 0 to 0.2 kg s^{-1}. The oscillations in the inlet water flow were effectively suppressed using a flow control valve installed upstream of the test section. The maximum uncertainty in the measured water inlet flow rate was about 8% at the lower water flow rates and decreased to less than 2% at higher flow rates. Also, the maximum uncertainty in the calculated equilibrium exit quality was about 5%, and it decreased as the exit quality increased, reaching less than 1% at the highest exit quality of approximately 48%. The uncertainties in the experimental measurements were determined by the method of Kline and McClintock [17].

In the experiments, the CHF was determined when a surge in the wall temperature past 473 K and/or a

bright glow was observed near the top of the heated length. To protect the heated tube from physical burnout during the CHF experiments, a power trip was installed between the test section and the power supply. This power trip was actuated by either of the two surface thermocouples located at 1 and 3 cm from the top of the heated tube. More details on the experimental setup and conduct are available elsewhere [18].

EXPERIMENTAL CONDUCT

The CHF experiments were conducted using deionized water (<20 p.p.m. mineral content) to avoid mineral deposits on the heater's surface. During the experiments, the pressure at the test section outlet was kept constant at 0.118 MPa by maintaining a constant water level in the overhead tank. To study the effect of the inlet subcooling on CHF, the inlet water temperature to the lower header was kept constant at one of three selected values, 298, 308 and 318 K; for each value, the coolant mass flux was varied from 0 to 260 kg m^{-2} s^{-1}. However, the water enthalpy at the bottom of the heated section was determined from the inlet subcooling after accounting for the temperature rise due to the heat generated in the brass tube and the copper conductor located at the bottom of the stainless steel tube. As a result despite the water temperature at the entrance of the annulus being kept constant, the inlet enthalpy at the bottom of the heated section varied with the water mass flux.

After adjusting the power trip and setting the water flow and inlet subcooling at the desired values, the electric power to the test section was increased gradually until incipient chugging at the top of the annulus was observed. Subsequently, the power was raised in increments of 100–200 W each; however, at each power level, the measured parameters were allowed to stabilize before raising the power level again. This process continued until CHF occurred. Each CHF experiment was conducted at least twice at the same water inlet flow rate and subcooling; the CHF values were generally reproducible to within $\pm 1\%$. As indicated earlier, the flow oscillations at the inlet of the test section were effectively suppressed by a throttle valve installed upstream of the test section.

EXPERIMENTAL RESULTS

A total of 383 CHF data were collected for the annulus ratios of 1.575, 1.72 and 2.0, covering inlet water subcooling ranging from 182 kJ kg^{-1} (44 K) to 312 kJ kg^{-1} (75 K) and water mass flux from 0 to 260 kg m^{-2} s^{-1}. The CHF data collected for the three annuli were plotted against the water mass flux in Fig. 1. As this figure shows, the CHF values varied from 155 kW m^{-2} for zero flow to a maximum of 1418 kW m^{-2} at a mass flux of 260 kg m^{-2} s^{-1}. Figure 1 also indicates that the CHF values increased as the water mass flux and/or inlet subcooling increased. Although the effect of water subcooling on the CHF was indistinguishable in the smaller annuli ($\varepsilon = 1.575$ and 1.72), and also in the largest annulus ($\varepsilon = 2.0$) for mass fluxes less than 140 kg m^{-2} s^{-1}, in the larger

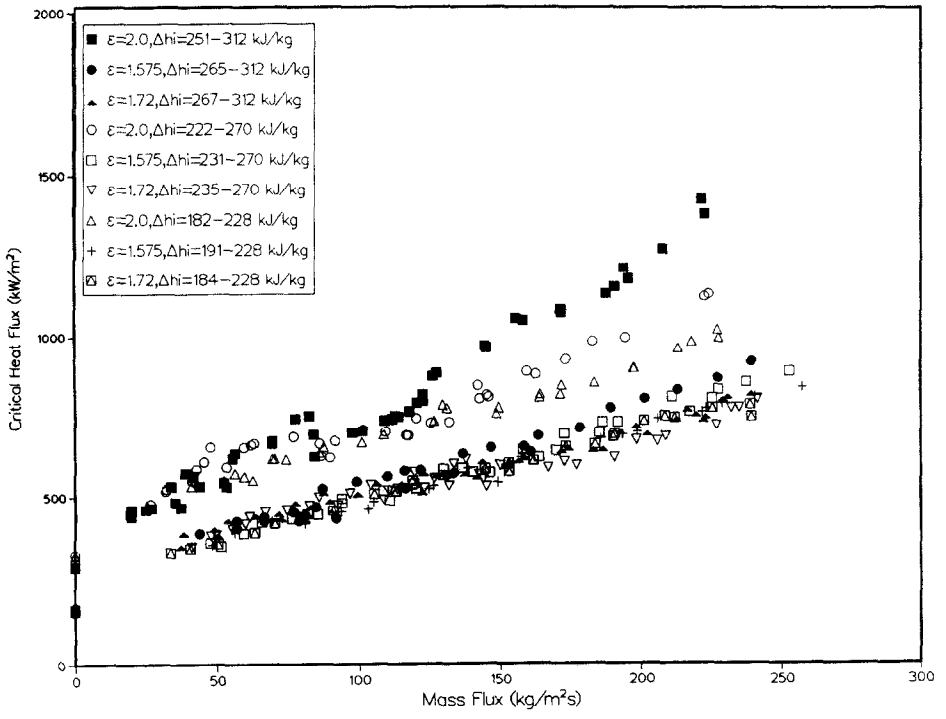

FIG. 1. Experimental CHF data for water flow in vertical annuli with annulus ratios of 1.575, 1.72, and 2.0.

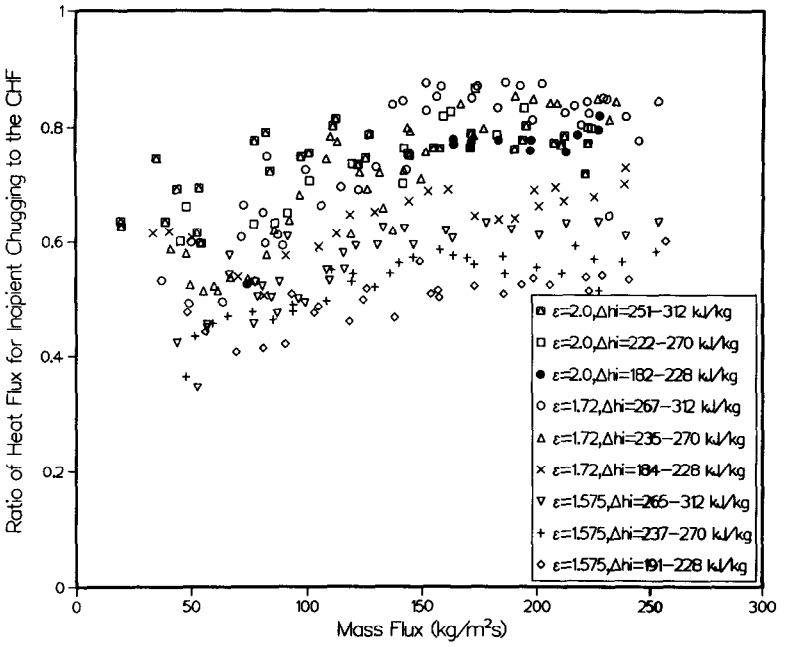

FIG. 2. Heat flux ratio for incipient chugging as a function of the water mass flux and annulus ratio.

annulus at mass fluxes greater than 140 kg m^{-2} s^{-1} CHF values increased as water inlet subcooling was increased. The results in Fig. 1 suggest that in the small annuli ($\varepsilon = 1.575$ and 1.72), the values of the water mass flux at which inlet subcooling begins to strongly affect CHF would be higher than 260 kg m^{-2} s^{-1}. Figure 1 also demonstrates that the CHF values with zero flow were about 30% lower than those with net water upflow when extrapolated to zero flow. This difference stems from the fact that while the CHF phenomenon for zero flow is controlled by the water flooding [14] from the exit of the test section, the CHF phenomena with inlet water flow depends on the flow hydrodynamics in the annulus at CHF.

In the experiments, the heat flux at incipient chugging was also measured. Because the oscillations in the inlet water flow were effectively suppressed in the experiments, flow chugging was characterized by successive water excursions that were driven by large vapor slugs through the top of the test section. Although the measured heat flux at incipient chugging (HFIC) is specific to the characteristics of the present experimental loop, the results demonstrate the effects of water inlet subcooling and annulus ratio on the flow hydrodynamics in the test section prior to CHF.

As shown in Fig. 2, the heat flux at incipient flow chugging varied between about 40% of CHF for the smallest annulus ($\varepsilon = 1.575$) to 88% for the two larger annuli ($\varepsilon = 1.75, 2.0$); the difference depended on the water mass flux and inlet subcooling. As indicated in this figure, for a given mass flux the HFIC increased as the inlet subcooling and/or the annulus ratio increased. The HFIC, however, increased as the water mass flux increased up to approximately 150 kg m^{-2} s^{-1}. Beyond this point, the HFIC became almost independent of the mass flux, but increased as inlet subcooling and/or annulus ratio increased. These results suggest that at the same water mass flux, the large voiding of the flow channel caused earlier flow chugging and lower CHF values in the smallest annulus, than in the larger ones. However, increasing the water mass flux and/or inlet subcooling reduced the voiding of the channels, and thus increased both the HFIC and the CHF. At mass fluxes beyond 150 kg m^{-2} s^{-1}, the equilibrium exit quality became very small (<1%), and almost independent of the mass flux (Figs. 8 and 9). Also, the values of HFIC became independent of the water mass flux, but increased as inlet subcooling increased.

Visual observations and the video images of the flow field in the experiments also indicated that the frequency and the intensity of the water chugging as well as the extent of the vapor slugs within the annular gap decreased as the coolant mass flux increased. When the heat flux was high enough to evaporate the water film at the top of the heated tube before the heater surface was rewetted by the water, CHF occurred. As indicated in this section, the flow transition at CHF varied as a function of the annulus ratio and the equilibrium exit quality.

The present CHF data for the three annulus ratios, excluding those for zero flow, were classified using the criteria of Ishii and Mishima [15] according to the flow transitions which occurred at CHF: the slug–churn flow transition, the churn–annular flow transition and the annular–annular mist flow transition. The flow transition at CHF was identified based on the recorded video images and the still photographs of the flow fields at CHF as well as by plotting the CHF values vs the equilibrium vapor quality on a

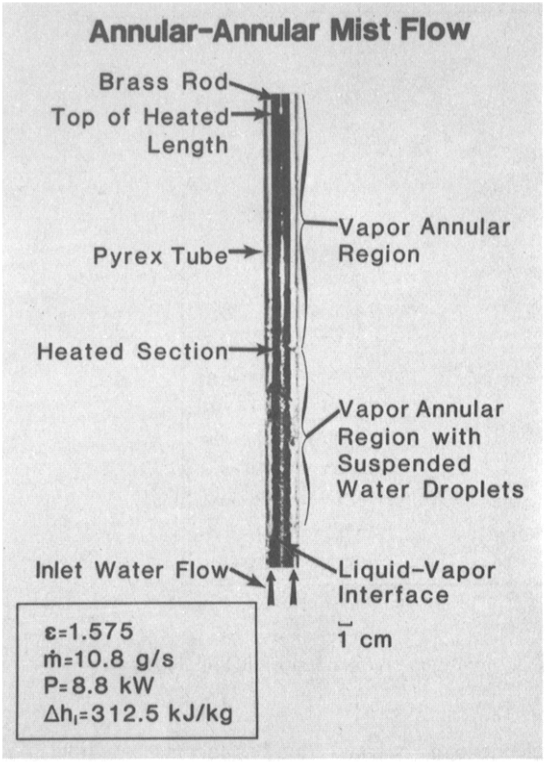

FIG. 3. Pictorial image of annular–annular mist flow transition for an annulus ratio of 1.575.

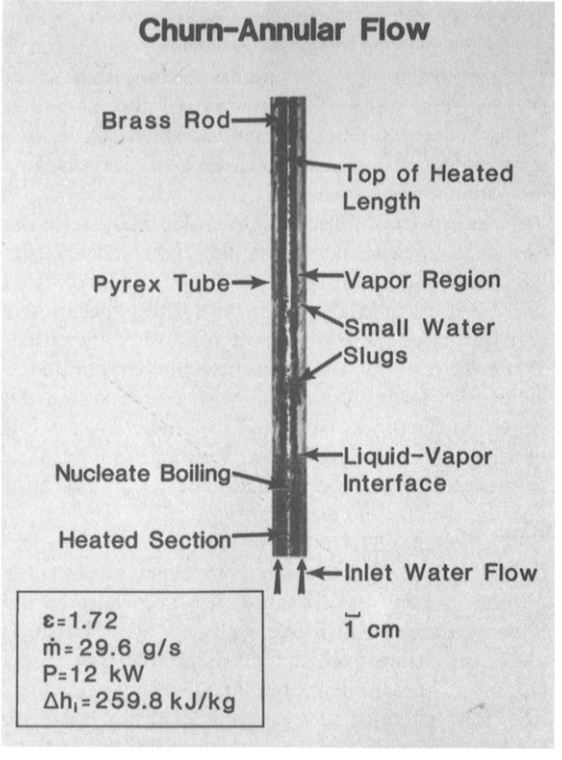

FIG. 4. Pictorial image of churn–annular flow transition for annulus ratio of 1.72.

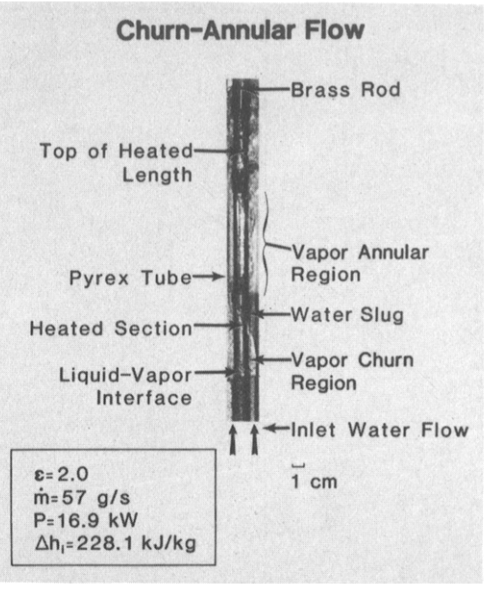

FIG. 5. Pictorial image of churn–annular flow transition for an annulus ratio of 2.0.

two-phase flow map [19]. Figures 3–6 present pictorial images of the flow transitions typical of those which occurred at CHF. Figures 7–9 present the CHF data plotted onto two-phase flow maps for the annulus ratios 1.575, 1.72, and 2.0, respectively. While all the CHF data for the smallest annulus ($\varepsilon = 1.575$) were parallel and close to the annular–annular mist flow transition line, the data for the two larger annuli occurred in the slug, churn and annular flow regimes. In Figs. 7–9 the deviation between the data and the theoretical boundaries as well as the spread of the data between the various flow regimes at low vapor quality may be attributed in part to the fact that the

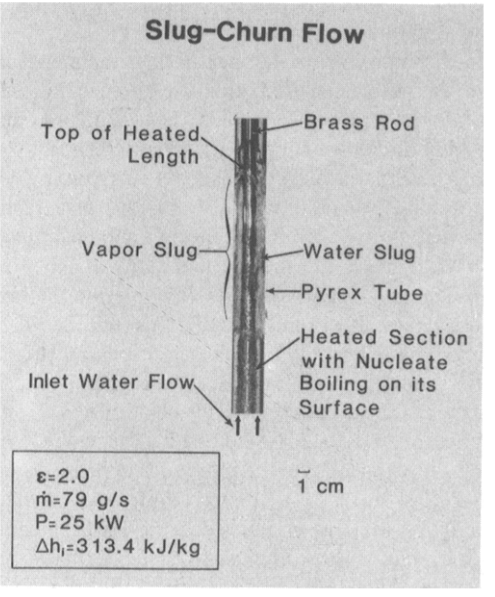

FIG. 6. Pictorial image of slug–churn flow transition for an annulus ratio of 2.0.

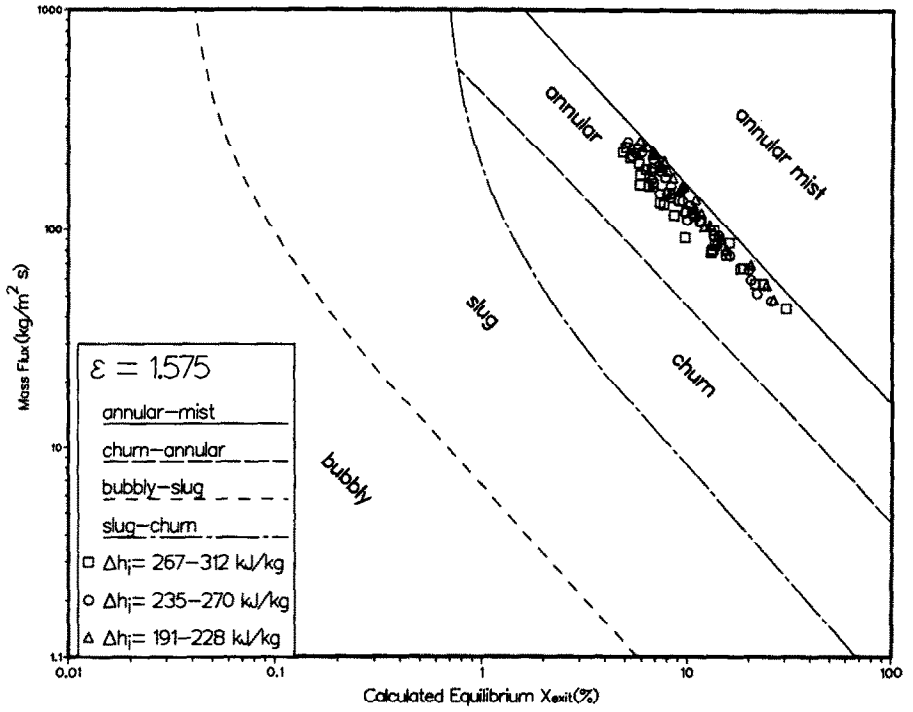

FIG. 7. Experimental CHF data for an annulus ratio of 1.575 plotted on a two-phase flow map.

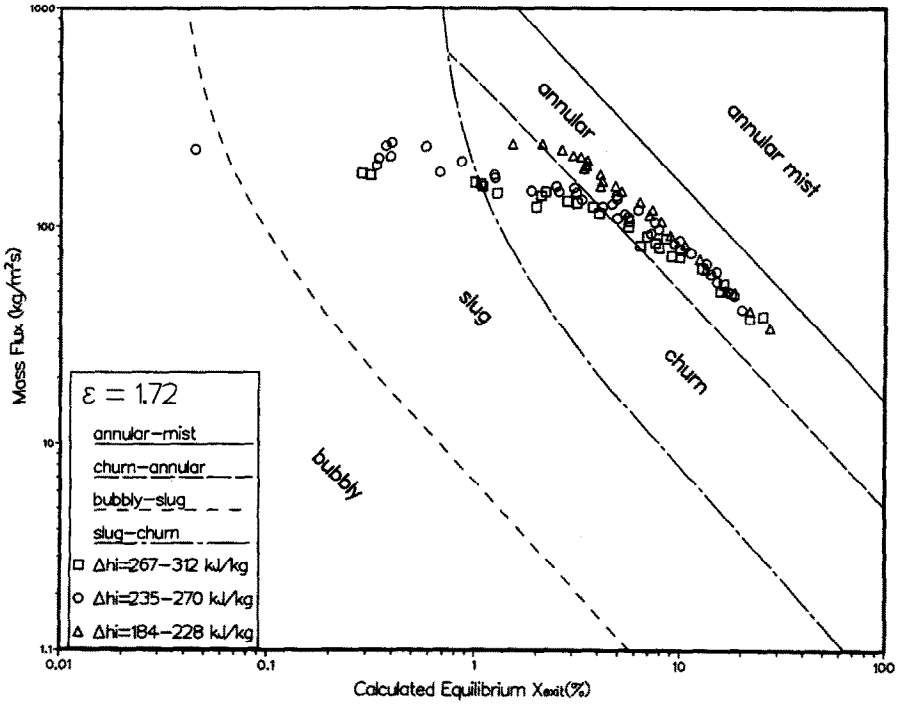

FIG. 8. Adiabatic two-phase flow map for an annulus ratio of 1.72 with CHF experimental data.

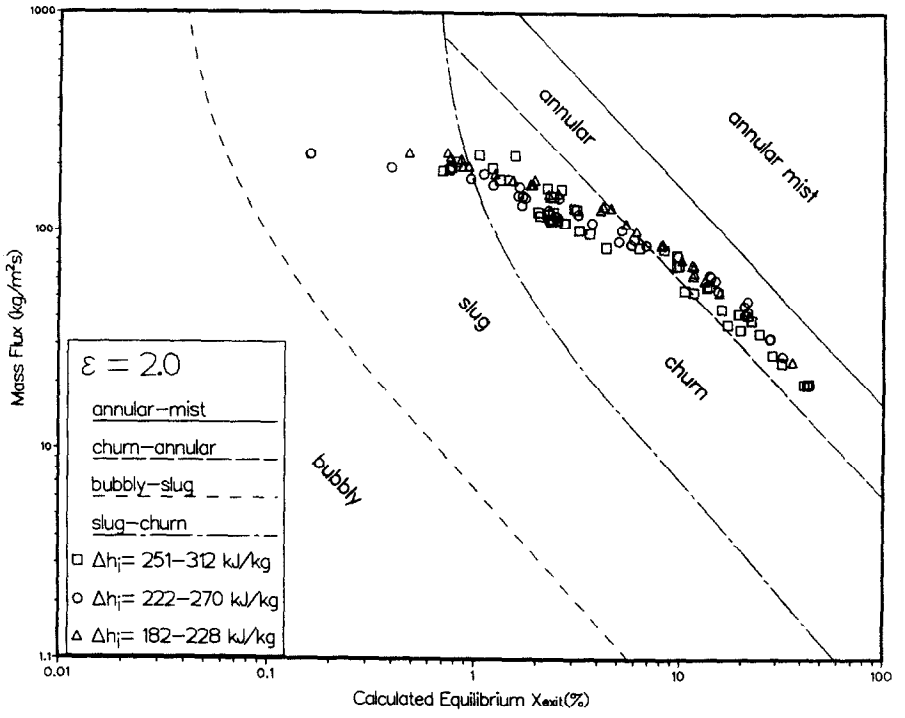

FIG. 9. Experimental CHF data for an annulus ratio of 2.0 plotted on a two-phase flow map.

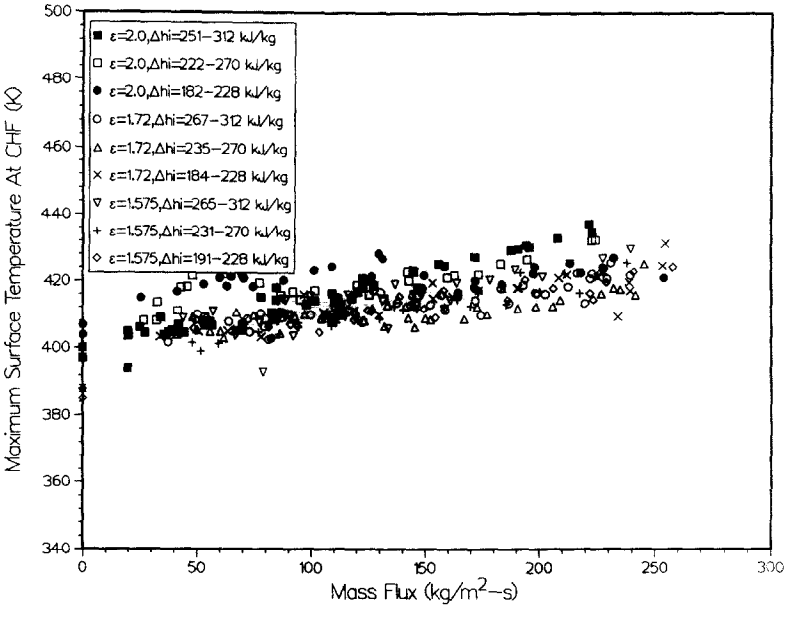

FIG. 10. Maximum surface temperature at CHF as a function of water mass flux and annulus ratio.

equilibrium exit quality, instead of the actual vapor quality, was used to develop the maps.

As Fig. 10 demonstrates, the heater surface temperature at CHF was almost independent of the annulus ratio and of the water inlet subcooling but increased as the water mass flow rate increased; it varied only from 400 to 430 K as the coolant mass flux was increased from about 10 to 260 kg m^{-2} s^{-1}. For zero net flow conditions, however, the heater maximum surface temperature was lower and strongly dependent on the size of the annulus; it varied from 380 to 408 K for annulus ratios of 1.575 and 2.0, respectively.

In the zero flow experiments, the upper portion of the heater was cooled directly by the downward flow of water, while the lower portion of the heater was cooled by the water supplied by the downward flow through the film along the inner surface of the outer Pyrex tube. This simultaneous cooling of the upper and lower portions of the heater produced maximum

voiding of the flow channel near the middle of the heater's length; it also caused the water film on the heater surface to dryout, thus causing CHF to occur at this location. In the following section, the CHF data are analyzed and correlated.

DEVELOPMENT OF CRITICAL HEAT FLUX CORRELATIONS

The heat balance equation in the heated test section at the CHF was used to develop the following dimensionless expression for CHF [15]:

$$q^*\left(\frac{A_h}{A}\right)=\left[\sqrt{\left(\frac{\rho_v}{\lambda g\Delta\rho}\right)}j_v+\frac{\Delta h_i}{h_{fg}}G^*\right] \quad (1)$$

where

$$q^*=Q/h_{fg}A_h\sqrt{(\lambda\rho_v g\Delta\rho)}$$
$$G^*=G/\sqrt{(\lambda\rho_v g\Delta\rho)}$$
$$\lambda=\sqrt{(\sigma/g\Delta\rho)}. \quad (2)$$

Note that the term $j_v(\rho_v/\lambda g\Delta\rho)^{1/2}$ in equation (1) strongly depends on the void fraction distribution in the annular gap as well as on the flow transition occurring at CHF, rather than on the coolant mass flux. At the transition from churn to annular flow in vertical tubes, this term is given as [16, 19]

$$j_v\left(\frac{\rho_v}{\lambda g\Delta\rho}\right)^{1/2}=\left(\frac{1}{Co}-0.11\right) \quad (3)$$

where the void distribution parameter Co at the location of CHF is given as

$$Co=1.2-0.2\sqrt{\left(\frac{\rho_v}{\rho_f}\right)}. \quad (4)$$

In annuli, unlike the flow in vertical tubes, the largest concentration of the bubbles would not occur in the middle of the annular gap; thus, the value of Co may be different from that given by equation (4). Also, the value of Co in a boiling channel is not constant but varies with position as the void and velocity profiles develop. Because of the uncertainty associated with determining the correct expression for Co for flow in vertical annuli, equation (1) was rewritten in the following empirical form which also includes the effect of the aspect ratio, L/D_{eh}:

$$q^*\left(\frac{A_h}{A}\right)=A_1\left[\frac{L}{D_{eh}}\right]^{B_1}\left[C_1+D_1\frac{G^*\Delta h_i}{h_{fg}}\right] \quad (5)$$

where the coefficients A_1, B_1, C_1, and D_1 were determined from the least square fit of equation (5) to the CHF data for both the slug–churn and the churn–annular flow transitions: $A_1=1.65$, $B_1=0.2$, $C_1=0.933$ and $D_1=0.212$. As Fig. 11 demonstrates, equation (5) is in good agreement with the CHF data; the deviation between the data and the correlation is within $\pm 15\%$. Figure 12 demonstrates that while the dependency of the CHF on the (L/D_{eh}) is consistent with the data reported previously by Rogers *et al.* [13] for mass fluxes less than 250 kg m^{-2} s^{-1}, it is significantly higher than that indicated by the data of

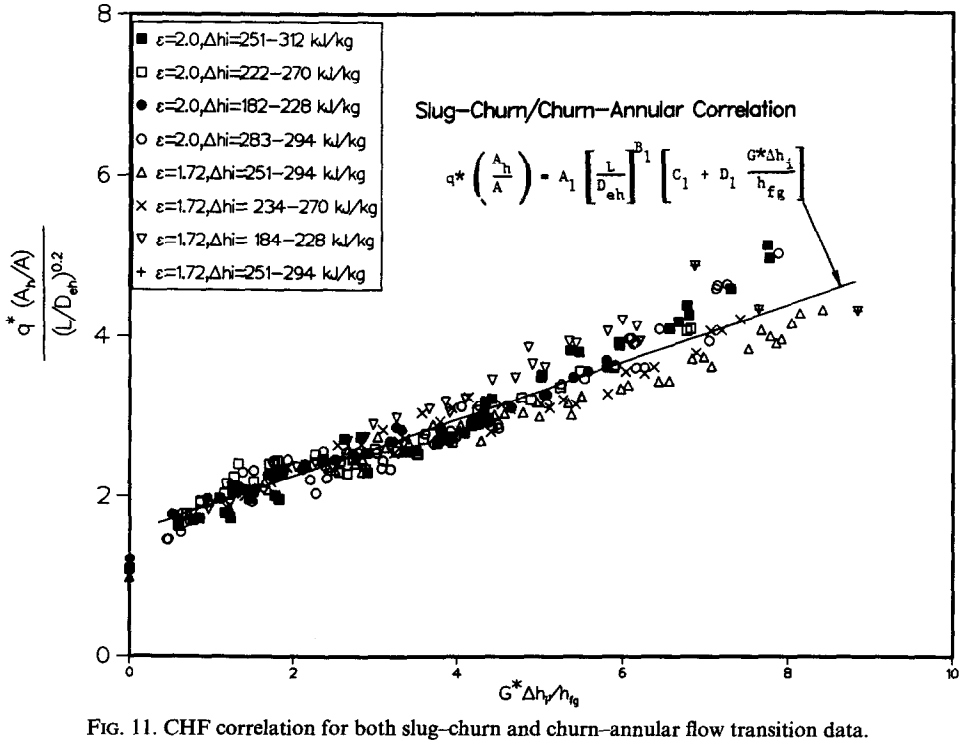

FIG. 11. CHF correlation for both slug–churn and churn–annular flow transition data.

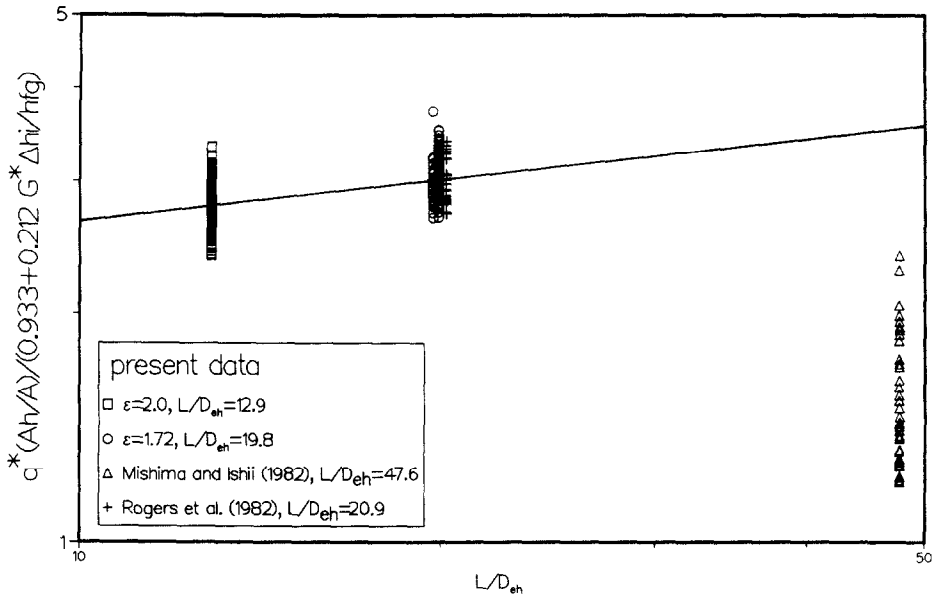

FIG. 12. Effect of L/D_{eh} on CHF in vertical annuli.

Mishima and Ishii [14] for mass flows less than 40 kg $m^{-2}\ s^{-1}$.

As shown earlier, the CHF in the smallest annulus ($\varepsilon = 1.575$) occurred at the transition from annular to annular mist flow. At this transition, the vapor velocity is high enough to cause entrainment of liquid droplets from the liquid film at the heater surface into the vapor flow. Based on the criterion for the onset of droplet entrainment by Ishii and Grolmes [16], the vapor velocity for a rough turbulent film flow of a weakly viscous fluid, such as water, can be given by

$$j_v = \left(\frac{\sigma g \Delta\rho}{\rho_v^2}\right)^{1/4} N_{\mu f}^{-0.2}. \tag{6}$$

The criterion given by equation (6) is recommended for a film Reynolds number, Re_f, greater than 1635. In the CHF experiments, Re_f was calculated based on the measured film thickness, δ_f, at the surface of the heater where CHF occurred. The thickness of this liquid film was determined from the video images of the flow field to be approximately 1.8 mm. The thickness of the liquid film at the inner surface of the outer Pyrex tube was about the same as that on the heater surface. Assuming the same average mass, velocity in both films, the film average Reynolds number can be given as

$$Re_f = \frac{4\Gamma}{\nu_f} \tag{7}$$

where

$$\Gamma = \frac{\rho_f \delta_f}{2} j_f. \tag{8}$$

The water velocity in the film, j_f, can be approximately given by

$$j_f = \frac{\dot{m}}{\rho_f \dfrac{\pi D^2}{4}\left[\left(1+\dfrac{\delta_f}{D_i}\right)^2 - 1 + \varepsilon^2\left\{1-\left(1-\dfrac{\delta_f}{\varepsilon D_i}\right)^2\right\}\right]} \tag{9}$$

In the CHF experiments with $\varepsilon = 1.575$, the calculated values of Re_f using equation (7) varied from 1860 to 9300. Since these values are significantly higher than 1635, equation (6) can then be used to predict the vapor velocity at the annular–annular mist flow transition.

Eliminating j_v between equations (1) and (6) gives the following empirical correlation for CHF at the annular–annular mist flow transition:

$$q^*\left(\frac{A_h}{A}\right) = \left[C_2 N_{\mu f}^{-0.2} + D_2 \frac{\Delta h_i}{h_{fg}} G^*\right] \tag{10}$$

where the coefficients C_2 and D_2 were determined from the least square fit of equation (10) to the CHF data; $C_2 = 0.85$ and $D_2 = 1.045$ (Fig. 13). Equation (10) is in excellent agreement with CHF data; the deviation between the data and this correlation is within 7 and −12%. Unlike equation (5), which compiles the data from two difference annuli ($L/D_{eh} = 12.86$ and 19.7) the dependence of CHF on L/D_{eh} in the smallest annulus was not quantified because the results are only for a single annulus ratio ($\varepsilon = 1.575$) with $L/D_{eh} = 26.1$.

COMPARISON WITH HIGH FLOW CHF CORRELATIONS

Figure 14 shows the comparison between equation (5) and the CHF correlations of Biasi *et al.* [8], Macbeth [9, 10] and Bernath [11]. As demonstrated in Fig.

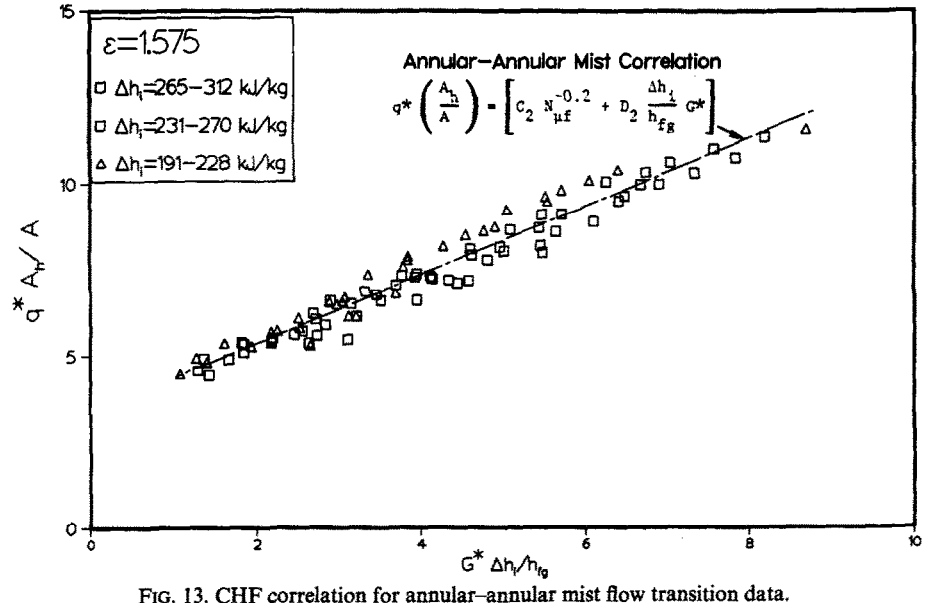

FIG. 13. CHF correlation for annular–annular mist flow transition data.

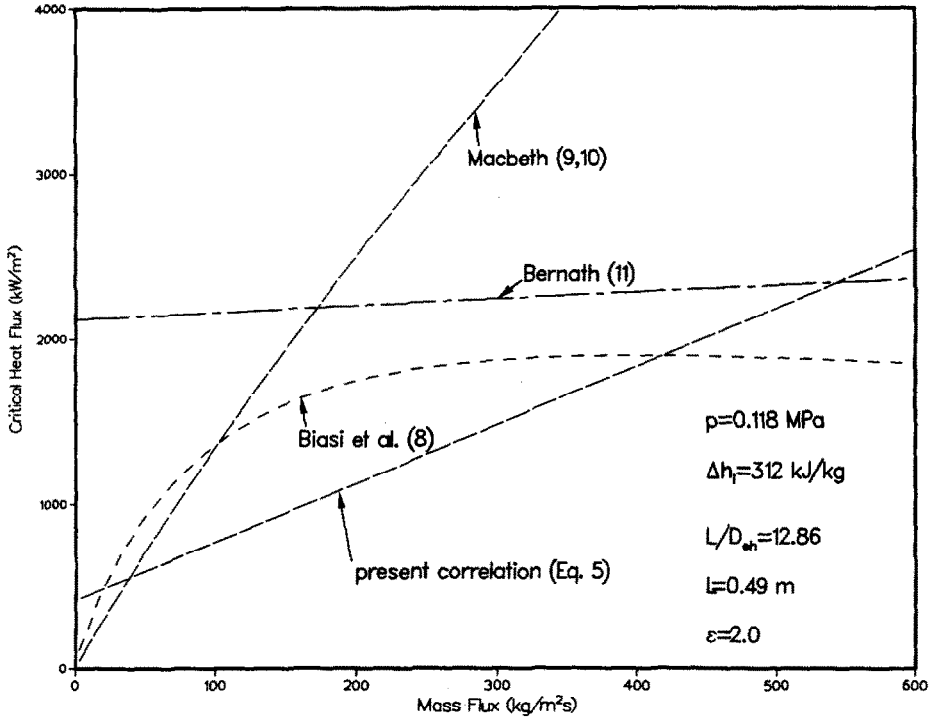

FIG. 14. Comparison of the present CHF correlation for slug–churn and churn–annular flow transitions with those of Bernath [11], Macbeth [9, 10], and Biasi *et al.* [8].

14, the correlations of both Biasi and Macbeth predict zero CHF values for zero flow conditions; this prediction is in contrast with the present experimental results (Fig. 1) and with those of Mishima and Ishii [14]. This difference stems from the fact that the Biasi and Macbeth correlations, although derived from CHF data covering a wide range of higher pressure and mass fluxes, were based on a limited low flow, low pressure data base. The Bernath correlation [11], however, does predict a positive value for CHF when extrapolated to zero flow conditions. Nonetheless, the predicted CHF value is much higher than those measured in the present work and those of Mishima and Ishii [14] for low water flow in vertical annuli. While the Bernath correlation predicts a CHF value of about 2100 kW m^{-2} at zero flow, the present experimental values varied from 155 to 336 kW m^{-2} for annulus ratios of 1.575–2.0, respectively. These results suggest

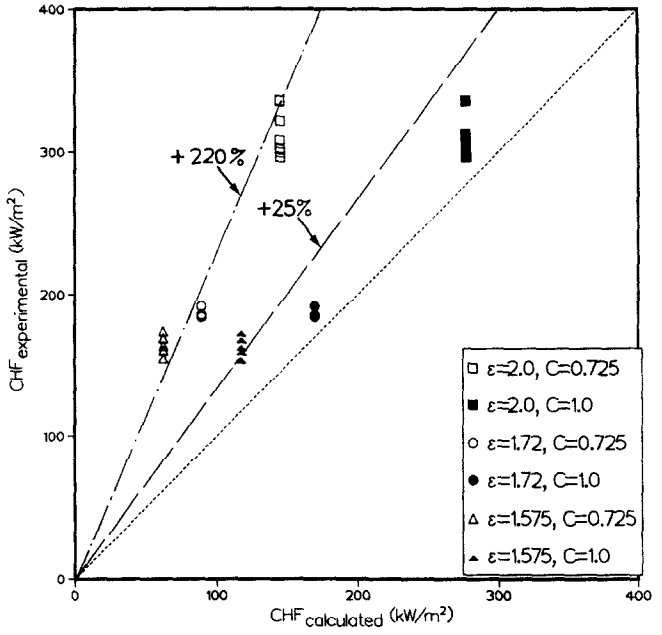

FIG. 15. Comparison of the zero flow CHF data with Block and Wallis' flooding correlation [20].

that the Bernath correlation, when extrapolated to low flow conditions, significantly overestimate the values of CHF. Similarly, at flow rates in excess of 260 kg m^{-2} s^{-1}, the present CHF correlation (equation (5)) should not be used since it will overestimate the values of the CHF.

CHF DATA FOR ZERO WATER FLOW

This section presents and correlates the zero flow CHF data. At zero flow, CHF phenomena were governed by the flooding of the heated tube by the water from the overhead tank. In this situation, the escaping vapor through the top of the test section prevented the water from readily wetting the heated tube. To verify these observations, the zero flow CHF values were compared with the flooding correlation by Block and Wallis [20]

$$Q = C^2 A h_{fg} \sqrt{(\rho_v g \Delta\rho D)} \left[1 + \left(\frac{\rho_v}{\rho_f}\right)^{1/4}\right]^2 \quad (11)$$

where C is a constant describing the entrance effects to the top of the test section. In the present experiments the hydraulic diameter for the annulus, D_e, was substituted for D in equation (11). For a vertical tube with a sharp edged entrance, C was given as 0.725; while for round edged entrances, C was given as 0.88–1.0. In the present experiments, the ends of the Pyrex tubes were thermally treated by an oxyhydrogen torch to smooth and round the edges of the tubes. Thus, the value of C was expected to be between 0.88 and 1.0. Figure 15 plots the CHF values for zero flow vs the predicted values using the Block and Wallis flooding correlation [20]. This figure shows that the CHF predictions using $C = 1.0$ gave the best comparison with measured CHF values; the deviation between the experimental values and the predictions was within 25%. This deviation is significantly lower than that for $C = 0.725$ (220%). These results confirm that the CHF values for zero flow could be reasonably predicted using the flooding criterion by Block and Wallis [20].

SUMMARY AND CONCLUSIONS

Critical heat flux experiments were conducted using vertical annuli (annulus ratios of 1.575, 1.72 and 2.0) at low flow of water and near atmospheric pressure (0.118 MPa). In these experiments, the effects of the annulus ratio and the water's mass flux and inlet subcooling on CHF as well as the flow transition at CHF were investigated. Results show that the CHF values increased as the water mass flux or annulus ratio increased. However, the effect of inlet subcooling on CHF was not distinguishable in the smaller annuli (annulus ratios of 1.575 and 1.72) and for the largest annulus (annulus ratio of 2.0) at water mass fluxes less than 140 kg m^{-2} s^{-1}. Conversely, in the largest annulus at higher mass fluxes, the data showed a distinct effect of inlet water subcooling on CHF; the CHF values increased as the inlet water subcooling increased. The results also showed that the CHF, which was of the dryout type, caused the liquid film at the top of the heated tube to evaporate resulting in an abrupt rise in the heater's surface temperature. At CHF, the heater's temperature varied within a narrow range and was generally independent of the annulus ratio; however, it increased as the water mass flux increased. The heat flux at incipient flow chugging in the flow channel also varied from a minimum of about

40% of the CHF values in the smallest annulus ($\varepsilon = 1.575$) to a maximum of approximately 88% of CHF in the large annuli ($\varepsilon = 1.72$ and 2.0); it also increased as either the water mass flux, inlet subcooling, or the annulus ratio increased.

The flow transition at CHF varied with the annulus ratio and the water mass flux. While CHF in the smallest annulus ($\varepsilon = 1.575$) always occurred at the transition from annular to annular mist flow, in the larger annuli ($\varepsilon = 1.72$ and 2.0), the CHF occurred either at the transition from churn to annular flow or from slug to churn flow. This study also developed two CHF correlations: one for the annular–annular mist flow transition data and the other for both the slug–churn and churn–annular flow transition data. Finally, a comparison of the experimental data with the Block and Wallis correlation confirmed that CHF values for zero water flow can be reasonably predicted (within 25%) using Block and Wallis' flooding correlation.

Acknowledgements—The authors gratefully acknowledge the financial support provided by Sandia National Laboratories and General Atomics Technologies. Sincere thanks to Mr Fabian Foushee of General Atomics Technologies, to Mr Marlin Aker and Mr Reuben Rubio of Sandia National Laboratories, and to Dr R. Nelson and Dr K. O. Pasamehmetoglu of Los Alamos National Laboratory for their valuable input and comments. Special acknowledgement is also given to Mr James Schulze of Sandia National Laboratories for his assistance in the design and fabrication of the test section, to Dr Galal M. Zaki of the Egyptian Atomic Energy Authority for his input in the design and setup of the experiments, and to Mr D. V. Rao, graduate student in the Department of Chemical and Nuclear Engineering for his comments and help with the final production of the figures.

REFERENCES

1. L. S. Tong, *Boiling Heat Transfer and Two-phase Flow*. Wiley, New York (1965).
2. G. F. Hewitt, Burnout. In *Handbook of Multiphase Systems* (Edited by G. Hetsroni). Hemisphere, New York (1982).
3. J. G. Collier, *Convective Boiling and Condensation*. McGraw-Hill, London (1972).
4. Y. Katto, Critical heat flux in boiling, *Proc. 8th Int. Heat Transfer Conf.*, Vol. 1, p. 171. American Society of Mechanical Engineers (1986).
5. P. B. Walley, P. Hutchinson and G. F. Hewitt, The calculation of critical heat flux in forced convection boiling, *Proc. 5th Int. Heat Transfer Conf.*, Vol. 4, B6.11. Japan Society of Mechanical Engineers (1974).
6. G. F. Hewitt and N. S. Hall-Taylor, *Annular Two-phase Flow*. Pergamon Press, New York (1970).
7. S. Levy, J. M. Healzer and D. Abdollahian, *Prediction of Critical Heat Flux for Annular Flow in Vertical Pipes*, Electric Power Research Institute Report EPRI NP-1619 (1980).
8. L. Biasi, G. C. Clerici, S. Garribba, R. Sala and A. Tozzi, Studies on burnout, Part 3—A new correlation for round ducts and uniform heating and its comparison with world data, *Energia Nucleare* **XIV**(9), 530–536 (September 1967).
9. R. V. Macbeth, Burnout analysis, Part 3—The low-velocity burnout regime, AEEW-R222 (April 1963).
10. R. V. Macbeth, Burnout analysis, Part 4—Application of a local conditions hypothesis to World data for uniformly heated round tubes and rectangular channels, AEEW-R267 (August 1963).
11. L. Bernath, A theory of local-boiling burnout and its application to existing data, *Chem. Engng Prog. Symp. Ser.* **56**(30), 95–116 (1960).
12. K. Mishima, K. Nishihara and I. Michiyoshi, Boiling burnout and flow instabilities in a round tube under atmospheric pressure, *Int. J. Heat Mass Transfer* **28**, 1115–1129 (1985).
13. J. T. Rogers, M. Salcudean and A. E. Tahir, Flow boiling critical heat fluxes for water in a vertical annulus at low pressure and velocities, *7th Int. Heat Transfer Conf.*, Vol. 4, pp. 339–344. Hemisphere, New York (1982).
14. K. Mishima and M. Ishii, Experimental study on natural convection boiling burnout in an annulus, *7th Int. Heat Transfer Conf.*, Vol. 4, pp. 309–314. Hemisphere, New York (1982).
15. M. Ishii and K. Mishima, Study of two-fluid model and interfacial area, NUREG/CR-1873, Argonne National Laboratory (1980).
16. M. Ishii and M. A. Grolmes, Inception criteria for droplet entrainment in two-phase concurrent film flow, *A.I.Ch.E. Jl* **21**(2), 308–318 (1975).
17. S. J. Kline and F. A. McClintock, Describing uncertainties in single-sample experiments, *Mech. Engr* 3 (January 1953).
18. S. J. Haynes, Experimental studies for critical heat flux at low flow of water near atmospheric pressure in vertical annuli, M.S. Thesis, University of New Mexico, Albuquerque, New Mexico (August 1987).
19. M. Ishii, One-dimensional drift-flux model and constitutive equations for relative motion between phases in various two-phase flow regimes, ANL-77-47, Argonne National Laboratory (1977).
20. J. A. Block and G. B. Wallis, Heat transfer and fluid flows limited by flooding, *A.I.Ch.E. Symp. Ser. No.* 174 **74**, 73–82 (1978).

ETUDE EXPERIMENTALE SUR LE FLUX THERMIQUE CRITIQUE POUR DES FAIBLES DEBITS D'EAU DANS DES ESPACES ANNULAIRES VERTICAUX, A LA PRESSION PRESQUE ATMOSPHERIQUE

Résumé—Des expériences sont conduites pour mesurer le flux thermique critique (CHF) pour des débits faibles d'eau dans des espaces annulaires verticaux et pour une pression presque atmosphérique (0,118 MPa). Les résultats sont collectés pour des sous-refroidissements d'eau à l'entrée allant de 44 K (ou 182 kJ kg^{-1}) à 75 K (ou 312 kJ kg^{-1}), des débits-masse depuis 0 jusqu'à 260 kg m^{-2} s^{-1}. Les valeurs de CHF varient entre 155 kW m^{-2} pour un débit nul à l'entrée et un maximum de 1418 kW m^{-2} pour un débit-masse de 260 kg m^{-2} s^{-1}. Les données sont classées et unifiées en tenant compte d'un écoulement de transition. Deux formules de CHF sont développées pour les transitions typiques. Le flux de chaleur à l'endroit de l'apparition des bouffées a été mesuré et il varie depuis un minimum de 40% environ des valeurs CHF pur le plus petit espace annulaire (rapport d'anneau = 1,575) jusqu'à un maximum d'environ 88% du CHF pour les plus grands espaces annulaires (rapport d'anneau = 1,72 et 2,0). Les résultats montrent aussi que le flux de chaleur dans cette zone augmente quand le débit-masse de l'eau ou le sous-refroidissement à l'entrée augmente. Les valeurs CHF pour un écoulement nul à l'entrée est prédit à ±25% avec la formule de Block et Wallis.

KRITISCHE WÄRMESTROMDICHTE BEI LANGSAM STRÖMENDEM WASSER IN EINEM SENKRECHTEN RINGKANAL NAHE UMGEBUNGSDRUCK

Zusammenfassung—Messungen zur Bestimmung der kritischen Wärmestromdichte (CHF) für langsam strömendes Wasser in einem senkrechten Ringkanal bei ungefähr Atmosphärendruck (0,118 MPa) werden vorgestellt. Es werden CHF-Werte für Eintrittsunterkühlungen von 44 K (oder 182 kJ kg^{-1}) bis 75 K (oder 312 kJ kg^{-1}) und Massenstromdichten von 0 bis 260 kg m^{-2} s^{-1} erhalten. Die CHF-Werte variieren von 155 kW m^{-2} für ruhende Strömung bis zu einem Maximum von 1418 kW m^{-2} bei einer Massenstromdichte von 260 kg m^{-2} s^{-1}. Die Werte werden gemäß dem Strömungsübergang bei CHF klassifiziert und korreliert. Es werden zwei CHF-Korrelationen dargestellt, eine für den Übergang Pfropfen-Schaumströmung und Schaum-Ringströmung und eine andere für den Übergang Ring-Ringnebelströmung. Die Wärmestromdichte beim Beginn des "Strömungspumpens" wird ebenfalls gemessen. Diese variiert von 40% der CHF-Werte beim engsten Ringkanal (Radienverhältnis 1,575) bis zu ungefähr 88% von CHF bei breiteren Ringkanälen (Radienverhältnis 1,72 und 2,0). Es zeigt sich, daß die Wärmestromdichte beim Beginn des "Strömungspumpens" mit zunehmender Massenstromdichte und Eintrittsunterkühlung wächst. Die CHF-Werte für ruhende Flüssigkeit werden mit der Korrelation von Block und Wallis für Flüssigkeitsstau bei Gegenströmung innerhalb ±25% widergegeben.

ЭКСПЕРИМЕНТАЛЬНОЕ ИССЛЕДОВАНИЕ КРИТИЧЕСКОГО ТЕПЛОВОГО ПОТОКА ПРИ ТЕЧЕНИИ С МАЛЫМИ РАСХОДАМИ ВОДЫ В ВЕРТИКАЛЬНЫХ КОЛЬЦЕВЫХ КАНАЛАХ ПРИ ДАВЛЕНИИ, БЛИЗКОМ К АТМОСФЕРНОМУ

Аннотация—Экспериментально измеряется критический тепловой поток (КТП) при течении с малыми расходами воды в вертикальных кольцевых каналах при давлении, близком к атмосферному (0,118 МПа). Данные по КТП определяются для изменения недогрева воды на входе от 44 К (или 182 кДж $кг^{-1}$) до 75 К (или 312 кДж $кг^{-1}$) и массовых потоков от нуля до 260 кг $м^{-2}$ $с^{-1}$. Значения КТП изменялись от 155 кВт $м^{-2}$ при отсутствии потока воды на входе до максимального значения 1418 кВт $м^{-2}$ при расходе 260 кг $м^{-2}$ $с^{-1}$. Данные по КТП классифицируются и обобщаются в соответствии с переходным режимом течения, встречающегося при КТП. Выведены два соотношения для КТП, одно для дисперсно-стержневого и дисперсно-кольцевого переходных режимов течения и другое для перехода от кольцевого к кольцевому режиму течения для дисперсного потока. Измерен также тепловой поток при начале завихрения течения и найдено, что он изменяется от минимального, составляющего около 40% от величин КТП в наименьших кольцевых зазорах (соотношение колец = 1,575), до максимального, составляющего приблизительно 88% от величин КТП в других, больших по размеру кольцевых зазорах (соотношение колец = 1,72 и 2,0). Результаты также показали, что тепловой поток при возникновении завихрения увеличивается, так как возрастает либо массовый поток воды, либо недогрев на входе. На основе обобщенного соотношения Блока и Уэллиса рассчитаны величины КТП при отсутствии потока на входе с точностью ± 25%.